A&A 531, A58 (2011)
DOI: 10.1051/0004-6361/201116843

Astronomy & Astrophysics

New X-ray observations of IQ Aurigae and α^2 Canum Venaticorum

Probing the magnetically channeled wind shock model in A0p stars

J. Robrade and J. H. M. M. Schmitt

Hamburger Sternwarte, Universität Hamburg, Gojenbergsweg 112, 21029 Hamburg, Germany
e-mail: jrobrade@hs.uni-hamburg.de

Received 7 March 2011 / Accepted 11 May 2011

ABSTRACT

Aims. We re-examine the scenario of X-ray emission from magnetically confined/channeled wind shocks (MCWS) for Ap/Bp stars, a model originally developed to explain the ROSAT detection of the A0p star IQ Aur.
Methods. We present new X-ray observations of the A0p stars α^2 CVn (*Chandra*) and IQ Aur (*XMM-Newton*) and discuss our findings in the context of X-ray generating mechanisms of magnetic, chemically peculiar intermediate mass stars.
Results. The X-ray luminosities of IQ Aur with $\log L_X = 29.6$ erg s^{-1} and α^2 CVn with $\log L_X \lesssim 26.0$ erg s^{-1} differ by at least three orders of magnitude, although both are A0p stars. By studying a sample of comparison stars, we find that X-ray emission is preferably generated by more massive objects such as IQ Aur. Besides a strong, cool plasma component, significant amounts of hot (>10 MK) plasma are present during the quasi-quiescent phase of IQ Aur; moreover, diagnostics of the UV sensitive f/i line ratio in He-like O VII triplet point to X-ray emitting regions well above the stellar surface of IQ Aur. In addition we detect a large flare from IQ Aur with temperatures up to ~100 MK and a peak X-ray luminosity of $\log L_X \approx 31.5$ erg s^{-1}. The flare, showing a fast rise and e-folding decay time of less than half an hour, originates in a fairly compact structure and is accompanied by a significant metallicity increase. The X-ray properties of IQ Aur cannot be described by wind shocks only and require the presence of magnetic reconnection. This is most evident in the, to our knowledge, first X-ray flare reported from an A0p star.
Conclusions. Our study indicates that the occurrence the of X-ray emission in A0p stars generated by magnetically channeled wind shocks depends on stellar properties such as luminosity, which promote a high mass loss rate, whereas magnetic field configuration and transient phenomena refine their appearance. While we cannot rule out unknown close companions, the X-ray emission from IQ Aur can be described consistently in the MCWS scenario, in which the very strong magnetic confinement of the stellar wind has led to the build-up of a rigidly rotating disk around the star, where magnetic reconnection and centrifugal breakout events occur.

Key words. stars: activity – stars: chemically peculiar – stars: individual: α^2 CVn – stars: individual: IQ Aur – X-rays: stars

1. Introduction

X-ray emission is found virtually everywhere among the population of the main-sequence stars. However, for "hot" O and early-B stars, and "cool", late-A to M-type stars the X-ray generating mechanisms differ. In hot stars the correlation between X-ray and bolometric luminosity at $\log L_X/L_{bol} \approx -7$ (Berghoefer et al. 1997) is explained by X-ray emission arising from shocks in instabilities in their radiatively driven winds. In cool stars, X-ray emission originates in magnetic structures generated by dynamo processes, powered by an interplay of convective motions in the outer layers and stellar rotation. The observed activity levels range from $\log L_X/L_{bol} \approx -7 \ldots -3$ (Schmitt 1997), whereas an activity-rotation relation is present until the dynamo saturates (for an overview on stellar coronae see Güdel 2004). In intermediate mass stars, around spectral type late-A, the outer convection zone becomes increasingly thinner and the dynamo efficiency strongly declines. A prominent example is the A7 star Altair, one of the hottest magnetically active stars detected in X-rays (Robrade & Schmitt 2009). Thus one expects a virtually X-ray dark population at spectral types mid-B to mid-A, where stars neither possess an outer convection zone nor drive strong stellar winds. The overall X-ray detection rate among those stars is with ~10% quite low indeed, but surprisingly, X-ray emission was detected from several of these stars (Schröder & Schmitt 2007). Consequently, low-mass stars hidden in the vicinity of their optically bright primaries have often been proposed as the true origin of the X-ray emission. Unresolved companions are a likely explanation for the X-ray emission from "normal" main-sequence stars at these spectral types and in some cases they can even be shown to be responsible for the X-ray emission, e.g. in the eclipsing binary systems like α CrB (Schmitt & Kürster 1993). However, especially peculiar Ap/Bp stars and young Herbig AeBe stars are prime candidates for being intrinsic X-ray emitters (e.g. Babel & Montmerle 1997; Stelzer et al. 2009). In the Ap/Bp stars discussed here an interplay between stellar winds and large scale magnetic fields is thought to play the major role in the X-ray generation.

Ap/Bp stars are magnetic, chemically peculiar (CP) stars that have completed an often significant fraction of their main sequence lifetime, i.e., they are not particularly young. Only a small fraction of about 5% of the mid-B to mid-A type stars are magnetic; these stars typically exhibit various chemical peculiarities and a slower rotation compared to non-magnetic stars of similar spectral type. The origin of their magnetic field is debated, but often thought to be fossil, consistent with the finding that only a small fraction is magnetic and that field strength and rotation are independent. The magnetic field geometry in Ap/Bp stars is dominated by overall simple, large scale structures like a dipole and is hence fundamentally different from the complex field geometry of magnetically active late-type stars (see, e.g. the overview by Landstreet 1992).

The prototypical case for a presumably single, magnetic Ap star with detected X-ray emission is IQ Aur. In a 10 ks pointed observation with ROSAT PSPC, IQ Aur was shown to be an X-ray source with a high X-ray luminosity of $L_X = 4 \times 10^{29}$ erg s^{-1} and a quite soft spectrum with $T_X = 0.3$ keV (Babel & Montmerle 1997, BM97). These findings made a hypothetical late-type companion an unlikely explanation. To explain the X-ray emission from IQ Aur and more generally of Ap/Bp stars, BM97 introduced the "magnetically confined wind-shock model" (MCWS). In the MCWS model the radiatively driven wind components from both hemispheres of the star are magnetically confined and forced to collide in the vicinity of its equatorial plane. As a consequence, strong shocks form and give rise to very efficient X-ray production from kinetic wind energy. Although some fine-tuning is required to obtain a sufficiently high mass loss rate, the X-ray emission of IQ Aur can indeed be accounted for with reasonable assumptions on the wind parameters; specifically, BM97 assumed a stellar wind with $V_\infty = 800$ km s^{-1} and a mass loss rate of $\dot{M}_\odot = 10^{-10}$–10^{-11} $M_\odot$ yr^{-1}.

Notable advancements of the static BM97 model were achieved by magnetohydrodynamic (MHD) simulations of magnetically channeled line-driven stellar winds (ud-Doula & Owocki 2002). In a further study, the authors investigate an extended parameter space with these MHD simulations and include stellar rotation in the modeling (ud-Doula et al. 2008). Dynamic variants of the MCWS model were successfully applied to Herbig AeBe and O-type stars and may actually extend to a whole class of magnetic early-type stars. In this respect it can be considered as a "standard" model that is invoked to explain a variety of phenomena like X-ray overluminosity, hard spectral components, flares or rotational modulation. However, recent X-ray studies of Ap/Bp stars often remained inconclusive. Stelzer et al. (2006) studied X-ray detected intermediate mass main-sequence stars (B5-A0) with *Chandra* including three CP stars, but they do not find strong support for the MCWS model, especially because of the non-detection of the magnetic Ap star HD 133880. Czesla & Schmitt (2007) studied mid-B to mid-A magnetic stars; they detected X-ray emission from the A0p star GL Lac (Babcock's star), though with a much higher X-ray temperature and luminosity than IQ Aur, but also report the non-detection of the A0p star HD 184905. They find that the presence of a magnetic field is not a sufficient criterion for X-ray emission; moreover X-ray luminosity and field strength are not correlated.

These findings make it desirable to investigate the MCWS scenario in its "original" environment, and we present contemporary X-ray observations of two prototypical A0p stars, α^2 CVn and IQ Aur. Our paper is structured as follows: we summarize the target properties in Sect. 2, in Sect. 3 we describe observations and data analysis, present our findings in Sect. 4 and discuss them in a broader context in Sect. 5.

2. The targets α^2 CVn and IQ Aur

The A0p star α^2 CVn (HD 112413, HR 4915) is the primary component ($V = 2.9$) in a wide binary (angular separation 21.3″) with the F0V star HR 4914 as secondary. α^2 CVn is the prototype of a class of spectrum- and brightness-variable stars, whose variations are caused by the interplay of stellar rotation and starspots, i.e., metal inhomogeneities in the stellar atmosphere. These stars have spectral classifications from late-B to mid-A type and belong to the class of CP, magnetic stars. Kochukhov & Wade (2010) study spectropolarimetric data and find that the overall magnetic structure of α^2 CVn can be modeled with an 4.6 kG dipolar field, an inclination of $i \approx 120°$ and an obliquity, i.e., the angle between the rotational and the magnetic axes, of $\beta \approx 80°$. Nevertheless, higher complexity in the magnetic topology is also present. X-ray emission from this system was detected with *Einstein* (0.15–4.0 keV) at a level of $\log L_X = 28.8$ erg s^{-1} (Schmitt et al. 1985) and ROSAT (0.1–2.4 keV) at a level of $\log L_X = 28.6$ erg s^{-1} (Schröder & Schmitt 2007), but it was not resolved in both observations and the contribution from the individual components remained unknown.

Table 1. Basic properties of our targets.

Target	IQ Aur	α^2 CVn
X-ray obs.	XMM	Chandra-ACIS-S
Dist. (pc)	137	34
Sp.(chem) type	A0p – CP2, Si	A0p – CP2, Si EuHgCr
$\log L\,(L_\odot)$, $\log T$ (K)	2.5 ± 0.1, 4.16 ± 0.01	2.0 ± 0.1, 4.06 ± 0.02
$M\,(M_\odot)$, $R\,(R_\odot)$	4.0 ± 0.1, 2.9 ± 0.2	3.0 ± 0.1, 2.5 ± 0.3
$\log t$ (yr), τ (frac.)	7.8 (7.5–7.9), 0.4	8.3 (8.1–8.4), 0.52
$v \sin i$ (km s^{-1}), $P_{\rm rot}$ (d)	56, 2.47	18, 5.47
$B_{\rm eff}$ (kG)	0.74 ± 0.4	1.35 ± 0.4

The field A0p star IQ Aur (HD 34452, HR 1732) belongs to the class of α^2 CVn spectrum variable stars and is thought to be a single star with $V = 5.4$ and small $E_{B-V} \simeq 0.01$. Babel & Montmerle (1997), who report the ROSAT X-ray detection at $\log L_X = 29.6$ erg s^{-1}, assume a 4 kG dipolar field for IQ Aur and determine an inclination of $i \approx 32°$ and an obliquity of $\beta \approx 50°$, whereas Hubrig et al. (2007) find $i = 87°$ and of $\beta = 7°$. Bohlender et al. (1993) state: 'a large range of values for i is possible: if i is large β is fairly small and if i is as small as allowed by our assumptions, β may be more than 80°. The stellar parameter differ somewhat as well, e.g. BM97 assume $\log L/L_\odot = 2.9 \pm 0.2$, $M = 4.8\ M_\odot$, $R = 5.1 \pm 1.1\ R_\odot$ and $V_{\rm rot} = 105$ km s^{-1} whereas Hubrig et al. (2007) give $\log L/L_\odot = 2.3 \pm 0.1$, $M = 3.2 \pm 0.2\ M_\odot$, $R = 2.2 \pm 0.4\ R_\odot$ and $V_{\rm rot} = 46$ km s^{-1}. Because the adopted distance is the same, the stellar data and viewing geometry of IQ Aur appear to be only moderately constrained and time-variability might play an additional role. The values from Kochukhov & Bagnulo (2006), which are commonly used throughout our paper, are intermediate ones.

Both A0p stars are CP2 stars in the classification scheme of Preston (1974) and might be expected to be similar overall given their identical spectral type. However, IQ Aur is more luminous, more massive and younger than α^2 CVn. Indeed, IQ Aur is extreme for an A0p star; as a main-sequence star it would be of spectral type mid-B with its $B - V = -0.16$. The adopted basic stellar data for IQ Aur and α^2 CVn as compiled from Bohlender et al. (1993), Bychkov et al. (2003), Kochukhov & Bagnulo (2006) and Kochukhov & Wade (2010) are summarized in Table 1.

3. Observations and data analysis

We observed α^2 CVn in March 2009 with *Chandra* ACIS-S for 15 ks (Obs.ID 9923). The A0p star IQ Aur was observed in February 2010 with *XMM-Newton* for 115 ks (Obs.ID 0600320101) in the full frame mode with the thick filter inserted. Owing to the optical brightness of the target, the OM (optical monitor) had to be closed.

We used the software packages CIAO 4.2 and SAS 10 to process and analyze the data, applied standard selection criteria and utilize photons in the well calibrated energy ranges 0.2–

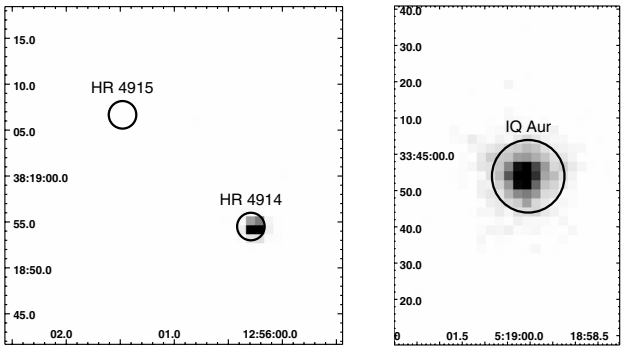

Fig. 1. *Left panel*: ACIS-S image of the α^2 CVn, the A0p star HR 4915 is X-ray dark. *Right panel*: MOS1 image of the A0p star IQ Aur. The circles denote the respective optical positions.

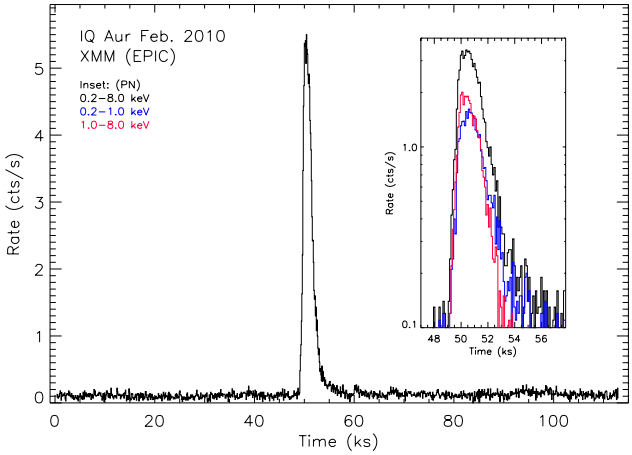

Fig. 2. X-ray light curve of IQ Aur from the summed EPIC data in the 0.2–8.0 keV band. *Inset*: the flare on a logarithmic scale in three energy bands as seen by the PN detector.

8.0 keV (*XMM-Newton*) and 0.3–8.0 keV (*Chandra*). For the spectral analysis of the *XMM-Newton* EPIC (European Photon Imaging Camera) data of IQ Aur source photons are extracted from a 30″ circular region around the source, the background is taken from nearby source-free regions on the MOS and the PN detectors respectively. The PN provides a higher sensitivity of the EPIC detectors, but the MOS provides a slightly better spatial and spectral resolution. The signal in the RGS (Reflection Grating Spectrometer) detectors is quite weak, therefore we extracted high-resolution RGS spectra from a 90% PSF source region and performed a cross-check with a narrower 70% PSF extraction area, in which the background is further suppressed. An additional problem are effective area drops in the RGS that affect, e.g., the region around the O VII intercombination line where several so-called "bad" channels lead to a reduced number of detected counts. To measure the line fluxes we used the fitting program CORA (Ness & Wichmann 2002), which accounts for these detector inhomogeneities.

We performed the spectral analysis of the EPIC/ACIS-S data with XSPEC V12.3 (Arnaud 1996). To model the spectra, we used photo-absorbed, multi-temperature APEC models with abundances relative to solar values as given by Grevesse & Sauval (1998), errors from spectral modeling denote 90% confidence level. We note that the interdependence of absorption, metallicity and emission measure ($EM = \int n_e n_H dV$) may result in different models of similar fit quality with the consequence that absolute abundances are more poorly constrained than abundance ratios or relative changes. The incomplete knowledge of atomic data used to calculate the spectral models also adds to these uncertainties, but they do not alter our main conclusions.

4. Results

Here we report on the results relevant to the origin of X-ray emission in Ap/Bp stars and present an analysis of the IQ Aur data, model its spectra, take a detailed look at the flare and investigate X-ray lines from the high-resolution spectrum.

4.1. Source detections, light curves, and a flare

The ACIS-S image of the α^2 CVn field, shown in Fig. 1, clearly reveals that the A0p star α^2 CVn (HR 4915) is X-ray dark. In the 0.3–3.0 keV band we detect no photon in a 2″ source region (95% PSF) centered on the expected optical position at an estimated background of 0.2 photons. We detect the F0 star HR 4914 with an X-ray luminosity of $\log L_X = 28.6$ erg s^{-1}, a quite typical value. For its position we find a small offset of about 0.5″ between the X-ray and expected optical position; nevertheless, applying a spatial correction to HR 4915 does not change the outcome. Adopting Poissonian statistics, we derive an 95% confidence upper limit of three counts for the source region. Assuming a plasma temperature of 0.3 (0.8) keV, this corresponds to an upper limit on the X-ray luminosity of $L_X < 0.6\ (1.0) \times 10^{26}$ erg s^{-1}, three to four orders of magnitude below the X-ray luminosity of IQ Aur ($L_X = 4 \times 10^{29}$ erg s^{-1}), although both are apparently similar stars. The flux limit for α^2 CVn converts into the by far the lowest upper limit obtained on the X-ray brightness for an A0p star.

In contrast, IQ Aur is detected in all *XMM-Newton* detectors; see the right panel of Fig. 1, where we show the MOS1 image. The derived X-ray position is about $\lesssim$1″ off from the expected optical position, a value within the positional uncertainty for *XMM-Newton*. To investigate the X-ray variability of IQ Aur, we extracted photons from a 35″ region (~90% encircled energy) around the X-ray source position on the EPIC detectors.

In Fig. 2 we show the background-subtracted light curve with 100 s time binning. Besides minor variability that is present throughout the observation, the X-ray count rate increases after 49 ks by a factor of roughly 40 within less than half an hour, the total flare event has a duration of about two hours. In the inset of Fig. 2 we show the light curve of the flare part as seen by the PN detector, also separated into a soft and hard energy band. The shape of the light curve with its fast rise time of 1000 s and e-folding decay time of ~1200–1400 s points to a single, relatively compact flaring structure. Because for X-ray emitting structures/loops the radiative energy loss scales with the square of the particle density, compact, i.e., small and dense structures radiate their energy much faster than larger tenuous structures of comparable X-ray luminosity. Moreover, the harder X-ray emission increases by a larger factor and its peak precedes that of the softer emission, a behavior that is reminiscent of coronal flares. We do not detect any spatial shift between the photons detected during the quasi-quiescent (QQ) and the flaring phase at an accuracy of $\lesssim$0.5″. In Fig. 3 we show the QQ part with two different time binnings. Notably, the average QQ X-ray count rate has increased by roughly 20% after the flare and the light curve shows slightly stronger variability, although the spectral hardness given by the ratio of the count rates in the 0.2–0.8 keV vs. 0.8–2.0 keV energy band is virtually identical compared to the pre-flare phase.

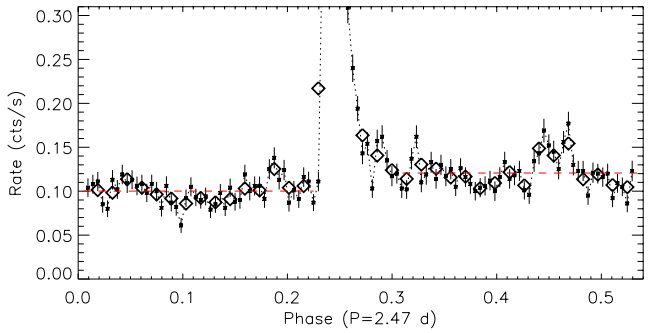

Fig. 3. Quasi-quiescent part of the X-ray light curve, phased with the rotation period of IQ Aur and binned to 1 ks (asterisks) and 3 ks (diamonds). The average rate before and after the flare is indicated by a red dashed line.

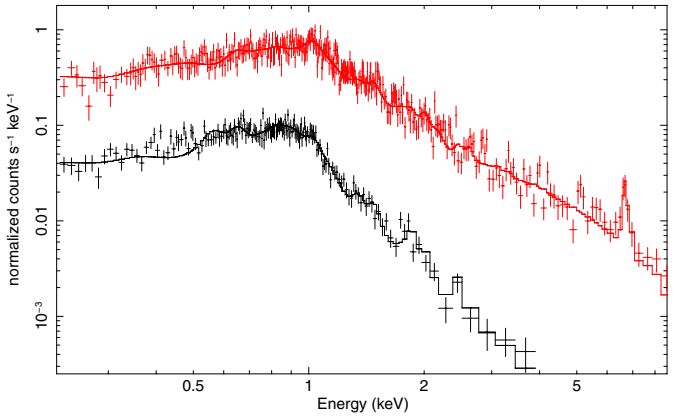

Fig. 4. XMM/PN spectra of the quasi-quiescent (black) and the flaring (red) phase with applied spectral models.

We see no strong modulation of the X-ray light curve that might be expected in an oblique rotator model ($P_{\rm rot}$ = 213 ks). Significant roughly sinusoidal shaped rotational modulation would be present if the star partially occults X-ray emitting material depending on rotational phase or when a disk around the star is viewed from different angles. An example are the X-ray brightness variations of the massive magnetic star θ^1 Ori C (Gagné et al. 2005). This model assumes cylindrical symmetry for the system as is likely appropriate for a star with a disk and as is commonly observed when, e.g. magnetic field variations are monitored, but clearly we cannot completely exclude unexpected phenomena during the phase that is not covered. Brightness variations on timescales of 20 ks (~0.1 phase) between consecutive bins during the pre-flare or the post-flare phase have an amplitude of $\lesssim$10% and appear mainly irregular. However, the strength of the modulation depends on the plasma location and the geometry of the system, and for a small obliquity the effects are likely minor in any case.

4.2. Spectral properties in quasi-quiescence

The global spectral properties of IQ Aur are determined from the EPIC spectra by using photo-absorbed multi-temperature models with free metallicity. Given the large variations in count rate over the observation, we separated the data into a flaring phase (PN: 49.1–58.1 ks) and a QQ phase for spectra analysis. As an example we show the respective PN spectra with the applied spectral models in Fig. 4; the derived spectral properties from our modeling are summarized in Table 2.

Table 2. Spectral models of IQ Aur (EPIC data).

Par.	QQ	Flare	Unit
$N_{\rm H}$	1.1 ± 0.9	1.0 ± 0.9	10^{20} cm^{-2}
Abund.	0.31 ± 0.08	0.67 ± 0.28	solar
T_1	0.26 ± 0.03	0.71 ± 0.09	keV
EM_1	1.75 ± 0.71	4.7 ± 2.0	10^{52} cm^{-3}
T_2	0.64 ± 0.15	1.59 ± 0.19	keV
EM_2	1.58 ± 0.56	14.4 ± 6.9	10^{52} cm^{-3}
T_3	1.10 ± 0.11	6.18 ± 1.46	keV
EM_3	1.88 ± 0.66	22.4 ± 7.1	10^{52} cm^{-3}
$\chi^2_{\rm red}$(d.o.f.)	1.09 (413)	0.97 (555)	
$L_{\rm X}$(em. 0.2–10.0 keV)	4.5×10^{29}	6.7×10^{30}	erg s^{-1}

The description of the QQ spectrum clearly requires the presence of additional hotter plasma components, besides the 0.3 keV component seen by ROSAT. Applying a one-temperature model,to the MOS spectra for example, results in an average temperature of kT = 0.75 keV, albeit with $\chi^2_{\rm red} > 2$ the fit is quite poor. Models with three temperature components describe the individual data sets well. The absorption component required to model the X-ray spectra of IQ Aur is quite weak, compatible with the findings from the ROSAT data. We again find strong emission from relatively cool plasma at ~3 MK (1 keV = 11.6 MK), but overall the plasma temperatures derived from the *XMM-Newton* spectra are significantly higher than those determined with ROSAT, where only weak indications for hotter plasma were found owing to the limited sensitivity of the instrument. We detect a significant contribution from $\gtrsim$10 MK plasma even in the QQ phase of IQ Aur, here it accounts for about 30% of the total emission measure. We find that a subsolar metallicity best describes the data. Using solar abundances reduces the emission measure, but also worsens the model quality ($\chi^2_{\rm red}$ = 1.24), albeit the temperature structure remains nearly identical. Allowing individual abundances to vary independently does not lead to robust results, therefore a global metallicity is used in all models. The best-fit model corresponds to a source flux of 1.7×10^{-13} erg cm^{-2} s^{-1} and an X-ray luminosity of $L_{\rm X} = 4.2 \times 10^{29}$ erg s^{-1} in the 0.2–2.0 keV band; for the ROSAT 0.1–2.4 keV band we derive a roughly 20% higher flux. This corresponds to an activity level of $\log L_{\rm X}/L_{\rm bol} \approx -6.4$, assuming that the X-rays are emitted by IQ Aur. Considering the ROSAT detection at a very similar X-ray luminosity of $L_{\rm X} = 4.0 \times 10^{29}$ erg s^{-1} nearly 15 years ago, IQ Aur has likely been emitting X-rays at a fairly constant level for more than a decade.

4.3. Global flare properties

During the flare phase, IQ Aur has not only significantly brightened, but as shown in Fig. 4 the associated spectrum is also much harder. The flare is most prominent at high temperatures, but strong excess emission is also present at lower temperatures. During the peak of the strong flare the emitted X-ray luminosity of IQ Aur rises to about $L_{\rm X} = 3.2 \times 10^{31}$ erg s^{-1} (0.2–10.0 keV), corresponding to a flux increase of nearly a factor 100 compared to the QQ state. With an average excess luminosity of $L_{\rm X} = 6.2 \times 10^{30}$ erg s^{-1} and a duration of 9000 s, the flare released about $E_{\rm X} = 5.6 \times 10^{34}$ erg only at soft X-ray energies. The flare emission is dominated by extremely hot plasma and even the average temperature is found to be around 45 MK. In the PN spectrum the prominent emission line complex from He-like Fe xxv is clearly visible at 6.7 keV, consistent with a hot

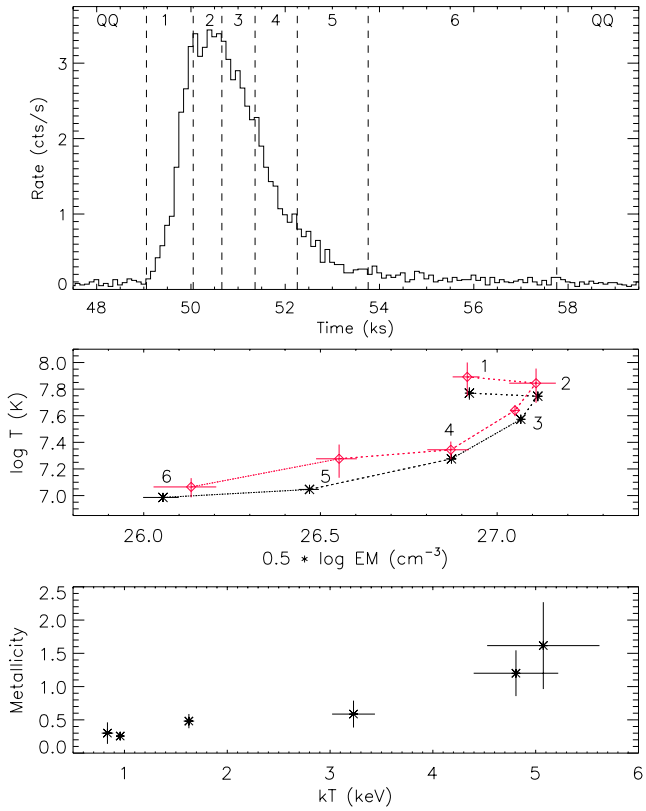

Fig. 5. Time-resolved study of the IQ Aur flare with XMM/PN data. *Top*: time intervals used in the analysis. *Middle*: temporal evolution of the plasma in the temperature/density plane (black/red: 1/2-T model). *Bottom*: metallicity vs. plasma temperature.

plasma component at temperatures of around 60–70 MK as deduced from the spectral model. Weak excess emission is present at the low-energy tail of this feature, that could be due to fluorescent emission from neutral iron from the Fe Kα line at 6.4 keV. However, formally the line is not detected at the 90% CL and its contribution to the X-ray flux is marginal at best with an equivalent width of $EW \lesssim 100$ eV. No significant changes in the absorption component are detected; in contrast, the metallicity of the flare plasma is found to be significantly higher than those of the QQ phase. While the absolute scale is only roughly constrained, we find a distinct metallicity trend, most noticeable when further separating the flare into individual time intervals as discussed in Sect. 4.4.

4.4. The flare under scrutiny

To study the evolution of the flare and its underlying structure in greater detail, we performed a time-resolved analysis for each of the six time segments as shown in the upper panel of Fig. 5. To derive the properties of the flare plasma (1–6), we added plasma components to the QQ model derived for the PN data. Here we use models with one or two temperature components and with or without metallicity as a free parameter to describe the flare plasma. The models lead to overall consistent results, see for example the time-evolution of the plasma properties presented in the middle panel of Fig. 5 for models with solar metallicity. The temperature given for the 2-T model is the emission measure weighted temperature. The flare reaches an X-ray brightness of about $\log L_X = 31.5$ erg s^{-1} and an average plasma temperature of around 80 MK around maximum, even roughly 100 MK plasma is present shortly after the impulsive heating during the rise phase (bin 1). The maximum temperature leads the maximum emission measure and thus in general the flare shows the temporal evolution of a typical coronal flare, i.e., a clock-wise turn in the temperature vs. density plane (see, e.g. Güdel 2004). Here the square-root of the emission measure is used as a density proxy, thus a fixed spatial extend of the X-ray emission region is assumed. While the initial decay is apparently steep, but only poorly constrained (bins 2–3), the flare evolution trajectory shows some flattening (bins 3–6) of the decay path. The origin of this behavior is unknown; it could be caused by minor re-heating events in the same structure or be produced by additional reconnection events in other magnetic structures that again might be triggered by the large flare. Another possibility is a change in size of the emitting region over the duration of the event.

Assuming a single, loop-like emitting structure, we can derive its size by adopting the formalism described in Reale et al. (1997) and parameters applicable to XMM/EPIC as given in Reale (2007). By using the maximum plasma temperature and the flare decay time obtained from the light curve, one can determine the size of the flaring structure, that is treated as an instantaneously heated coronal loop. Basically, one finds that $L \propto \tau_{lc} \sqrt{T_{max}}$, with L being the loop half-length, T_{max} the maximum plasma temperature and τ the decay time from the X-ray light curve and an additional scaling factor. This factor depends on the amount of additional heating during the decay, therefore one needs to estimate the importance of sustained heating. This is done by fitting the decay path derived from the one temperature model with a straight line to about about one tenth of the maximum intensity. This corresponds to bins 2–5 in the middle panel of Fig. 5, where we derive a slope of ~1 for the decay and consequently moderate re-heating has to be taken into account. Adopting the appropriate modeling parameter, i.e., $T_{obs} = 65$ MK, an e-folding decay time of $\tau = 1200$ s (measured to 1/10 of the maximum) and a correction factor for a slope of one, we obtain $L = 1.8 \times 10^{10}$ cm (0.1 R_*) for the loop half-length.

Because a coronal loop model might not be perfectly appropriate for IQ Aur and possible heating at later phases of the flare is only poorly constrained, we used as a conservative approach our most extreme values, i.e., 100 MK plasma temperature and 1400 s decay time and ignored ongoing heating. This method results in an upper limit for the size, and we derive $L \lesssim 3.5 \times 10^{10}$ cm (0.2 R_*) as maximum extent of the structure. While the flaring structure might be much smaller, even the upper limit corresponds to a moderately sized structure when compared to the stellar dimensions of IQ Aur. This finding excludes very large magnetic structures, e.g. from the global dipole, as the origin of the flare.

The IQ Aur flare is accompanied by a significant change in the metallicity of the X-ray emitting plasma as illustrated in the lower panel of Fig. 5 where we plot the results obtained from a 1-T model with metallicity as free parameter. During the impulsive phase of the flare as traced by the plasma temperature, more metal-rich material is heated to X-ray temperatures. The freshly heated plasma from the large flare exhibits solar or even slightly super-solar metallicity, which is a two to three times higher metallicity than the X-ray emitting plasma observed in the QQ phase. While the absolute scale is only moderately constrained, as outlined in Sect. 3, the relative changes are quite robust and also found in two temperature models or the analysis of the MOS spectra. In the final stages of the flare evolution, the remaining material has cooled down to temperatures below 1 keV, exhibits pre-flare metallicity and becomes

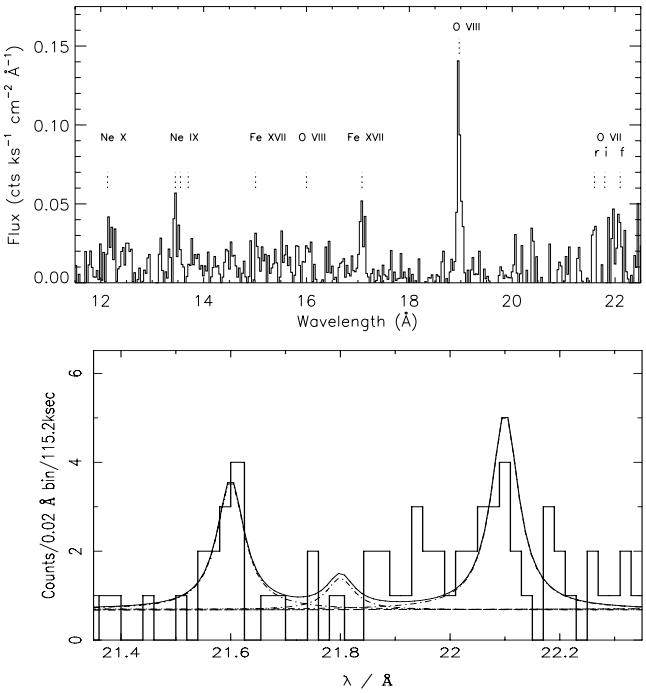

Fig. 6. High-resolution X-ray spectrum of IQ Aur. *Top*: total RGS 1+2 merged and flux-converted. *Bottom*: O VII triplet with model accounting for effective area inhomogeneities.

indistinguishable from the QQ plasma. Overall, we find a clear correlation between plasma temperature and metallicity, indicating a strong modification of the chemical composition during the event. Notably, the derived characteristics are quite typical for a stellar flare (see, e.g. Güdel 2004).

4.5. The high resolution X-ray spectrum

The high-resolution RGS spectrum from IQ Aur unfortunately has only a moderate signal-to-noise ratio (S/N) and only strong lines were clearly detected even in the total spectrum; see Fig. 6, where we show a flux-converted spectrum of the merged RGS detectors from a 90% PSF extraction region. The individual line fluxes were measured from the total count spectrum and cross-checked by using a broad and a narrower 70% PSF extraction region. The lower panel of Fig. 6 shows the O VII triplet with applied model, confirming that the forbidden line (22.1 Å) is significantly stronger than the intercombination line (21.8 Å). The S/N ratio is quite poor even in the total spectrum that includes the flare. We also investigated the QQ and flare phase separately, but except stronger emission from "hotter lines" (e.g. Fe XVII) during the flare, a quantitative comparison suffers from the low S/N. The fluxes of emission lines used in the subsequent analysis as determined from the total spectrum are given in Table 3. They are corrected for an absorbing column of $\log N_{\rm H} = 20$ cm^{-2} and we expect a flare contribution of roughly 30% to the given line fluxes.

We used the He-like O VII triplet to determine the distance of the X-ray emitting plasma to the surface of IQ Aur. O VII traces the location of plasma at temperatures around 2 MK, and its forbidden (f) to intercombination (i) line ratio is sensitive to density and UV radiation, specifically one finds $f/i = R_0/(1 + \phi/\phi_{\rm c} + n_{\rm e}/n_{\rm c})$, see, e.g. Mewe & Schrijver (1978); Porquet et al. (2001). In the low-density case ($n_{\rm e} \lesssim 10^{10}$ cm^{-3})

Table 3. Oxygen lines used in the analysis.

Ion/Line	Wavelength (Å)	Flux (10^{-15} erg cm^{-2} s^{-1})
O VIII	18.97	14.7 ± 2.3
O VII(r)	21.60	4.5 ± 1.9
O VII(i)	21.80	1.6 ± 1.2
O VII(f)	22.10	5.9 ± 1.9

additional photons in the i-line are only due to the radiation term $\phi/\phi_{\rm c}$. The radiation term describes the strength of the UV flux at 1630 Å and thus depends on the effective temperature and distance to the star. Using the fluxes in Table 3, we obtain $f/i = 3.7 \pm 3.0$, unfortunately the errors are relatively large. The ratio is consistent with virtually no radiation field being present ($R_0 = 3.95$), but much lower values are formally allowed as well. Adopting $f/i \gtrsim 1$, a photosphere with $T_{\rm eff} = 14\,450$ K and evaluating the radiation term, one finds that the X-ray emitting region is either shielded against the stellar UV-field or the X-rays originate predominantly from regions at $\gtrsim 7\ R_*$ above the surface of IQ Aur. As an alternative approach, we used the UV flux as measures by the IUE satellite and calculated $T_{\rm rad}$ from the observed spectrum. The 1630 Å UV flux from IQ Aur varies by a factor of nearly three over several years; using the lower flux measurements we find that the X-ray emitting region has to be located above the star at distances of $d \gtrsim 5\ R_*$. This result is independent of our assumptions; if higher densities are present, even larger distances to the stellar surface are required. Similarly, applying a correction for the weak extinction toward IQ Aur or adopting a higher UV flux would again shift the X-ray plasma location to larger distances. Therefore, we can virtually exclude X-ray emitting structure on or close to the star and thus the X-rays are produced at least several stellar radii above the surface of IQ Aur.

We also investigated the QQ and flare phase alone and found a similar high f/i-ratio for both cases, but with substantial error. Similarly, we studied the Ne IX-triplet and found an f/i ratio that is slightly higher but again fully consistent with the low density/no UV-field limit, but no additional information was gained regarding O VII. Further, we use the density constraint derived from the O VII f/i-ratio as a very rough cross-check on the size of the emitting volume. Adopting $f/i \gtrsim 1$ implies a density of $n_{\rm e} \lesssim 5 \times 10^{10}$ cm^{-3}, therefore we can now formally derive a minimum size of the emission region from this value. The average flare EM is 4×10^{53} cm^{-3} with $EM \approx 0.85\ n_{\rm e}^2 V$, from which one obtains for an emitting sphere a radius of $r \approx 0.14\ R_*$. We again found a comparatively small structure, in agreement with the estimation, i.e., $L < 0.2\ R_*$, derived from the above analysis of the flare.

By using the temperature-sensitive O VIII/O VII line ratios, we tested if additional cool plasma compared to pure coronal sources is produced by IQ Aur (see Fig. 7). The O VII lines form predominantly at temperatures around 2 MK, while O VIII traces hotter plasma at 3–5 MK. Additional O VII emission may be produced by accretion or wind shocks, as commonly observed in young T Tauri and Herbig AeBe stars, which generate relatively cool plasma compared to coronal sources of comparable X-ray brightness, see, e.g. Robrade & Schmitt (2007). The O VIII/O VII ratio measured for the QQ state IQ Aur is slightly below the values found for coronal sources, i.e., its X-ray emission is only moderately soft for its X-ray luminosity. However, it is well above the ratios found for HAeBe stars; young intermediate mass stars that drive outflows and jets with velocities of

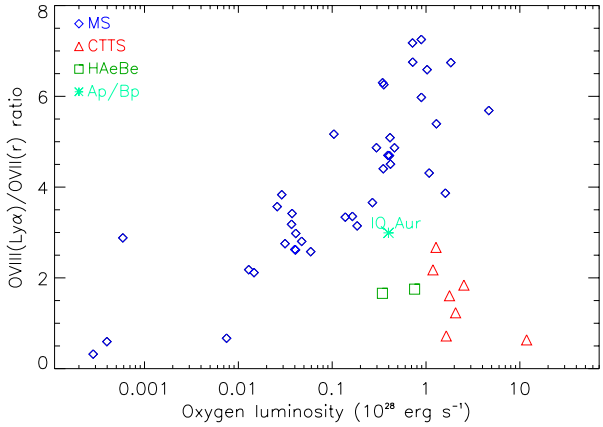

Fig. 7. Shown above is the quasi-quiescent O VIII/O VII ratio of IQ Aur, compared to accreting/wind driving young stars and main-sequence stars.

a few hundred km s^{-1}. These stars produce X-ray emission from predominantly cooler plasma, likely related to shocks in their outflows (Günther & Schmitt 2009).

5. Discussion

Our X-ray observations of the A0p stars IQ Aur and α^2 CVn present quite a complex X-ray picture. Here we discuss some implications imposed by our findings in the framework of the magnetically channeled wind shock (MCWS) scenario vs. a possible low-mass companion.

5.1. MCWS models for Ap/Bp stars

To detect MCWS generated X-ray emission from A0p stars, some basic conditions have to be fulfilled. The shock-speed has to be high enough to heat the plasma to X-ray emitting temperatures, the mass loss rate has be high enough to produce significant amounts of hot plasma to be detected with current instruments and a magnetic field configuration has to be present that effectively supports the conversion of kinetic wind energy to X-ray emission.

A key parameter in the dynamic MCWS model is the magnetic confinement parameter η_* (ud-Doula & Owocki 2002). It basically describes the ratio between the energy density of the magnetic field and the kinetic wind energy density and depends on stellar properties as given by $\eta_* \propto B_{\rm eq}^2 R_*^2/\dot{M}V_\infty$; here $B_{\rm eq}$ is the equatorial field strength, R_* the stellar radius, $\dot{M}$ the mass loss rate and V_∞ the terminal wind speed. Adopting values for IQ Aur, $B_{\rm eq} = 2$ kG, $R_* = 2.9\ R_\odot$, $\dot{M} = 10^{-11}\ M_\odot\,{\rm yr}^{-1}$ and $V_\infty = 700$ km s^{-1}, gives a confinement parameter on the order of $\eta_* \sim 10^6$. This value has significant uncertainty, but the requirements for strong confinement, i.e., $\eta_* \gg 1$, are definitely fulfilled. While at first analytic studies of rigidly rotating magnetospheres indicated that in the case of strong magnetic confinement an equatorial disk builds up from corotation radius outwards (Townsend & Owocki 2005), its formation is also present in MHD simulation when including effects of stellar rotation. These models predict the formation of a rigidly rotating disk by the accumulation of wind material, but episodes of infall and breakouts limit the build-up of the disk and lead to a dynamic but quasi-stationary behavior (ud-Doula et al. 2008); moreover the location of the temporary confined plasma around the equatorial plane can be estimated with the formalism presented in these works. For moderate rotation and very strong confinement the inner edge of disk is roughly given by the "associated Kepler-radius" $R_{\rm K} = W^{-2/3}$ with $W = V_{\rm rot}/V_{\rm orb}$ and $V_{\rm orb} = \sqrt{GM/R_*}$; using $V_{\rm rot} = 50$ km s^{-1} we obtain $R_{\rm K} \sim 5\ R_*$. The outer edge is determined by the extent of the closed magnetosphere $R_{\rm C} \approx 0.7\ R_{\rm A}$, slightly below the Alfvén radius given by $R_{\rm A} \approx \eta_*^{1/4} \times R_*$. For IQ Aur we obtain $R_{\rm A} \approx 30\ R_*$; clearly we are in a regime where $R_{\rm A} > R_{\rm K}$ and consequently the conditions required by the model for the formation of a rigid disk are fulfilled. The disk of IQ Aur is expected to be roughly located between ≈5–20 R_* and breakout events are mainly launched at distances of ≈20–30 R_*. We caution that these models assume an aligned dipole and were derived for more massive stars, thus an extrapolation to our Ap/Bp stars may not be straightforward. Nevertheless, the model is generally applicable for magnetically channeled line-drive stellar winds and therefore appears sufficient for the discussion of the overall phenomenology of X-ray emission presented below.

5.2. Why is IQ Aur X-ray bright and α^2 CVn X-ray dark?

The X-ray luminosity produced by MCWS follows the relation $L_{\rm X} \propto \dot{M}V_\infty B_*^{0.4}$, whereas the plasma temperature is given by $T_{\rm X} \approx 1.15 \times 10^5$ K $(V_{\rm sh}/100\ {\rm km\,s^{-1}})^2$ (BM97). Adopting similar wind speed and mass loss rate, one expects α^2 CVn to be comparably bright or even moderately X-ray brighter than IQ Aur. However, it is at least a factor thousand X-ray fainter than "expected" from the simplified assumption. This implies that either the mass loss rates differ by orders of magnitudes or that shock-speeds for α^2 CVn are so low, that the plasma does not reach X-ray temperatures. Because stellar wind speeds are likely comparable and strong confinement is achieved for both stars, a very low plasma temperature of $T_{\rm X} \lesssim 3 \times 10^5$ K as would be required to explain the tight upper limit on $L_{\rm X}$ for α^2 CVn, is virtually ruled out. It also appears unlikely that small differences in the magnetic topology of both stars lead to completely different wind channeling and wind shock configurations. A more reasonable explanations would be to propose a different mass loss rate and that IQ Aur differs by intrinsic properties that promote mass loss and thus X-ray generation, for example it is more luminous and hotter than α^2 CVn. In this case the X-ray generation would depend very sensitively on the underlying stellar parameter(s). Alternatively, the MCWS phenomenon could be a transient one and currently IQ Aur alone is in an active wind phase with a high mass loss rate. Unfortunately, mass loss rates of Ap stars usually cannot be independently measured, but are determined via modeling of, e.g. their X-ray properties. However, the strong wind phase is believed to be connected to abundance anomalies, which are also observed in α^2 CVn. It was already noticed by BM97 that any abundance anomalies should be removed by the relatively high mass loss rate, thus requiring that IQ Aur entered the active wind phase only recently, i.e., before a few Myr. Although the details of the onset of the strong wind phase are mainly unknown, BM97 estimate that Ap stars would spend a few percent of their lifetime in the strong wind phase, which would explain that most Ap stars are no X-ray sources, at least at the moment. Nevertheless, possibly even more prerequisites need to be fulfilled to make an A0p star a bright X-ray source.

5.3. X-rays from similar Ap/Bp stars

Given the very different findings for IQ Aur and α^2 CVn, we searched the *Chandra* and *XMM-Newton* archives for observations of similar Ap/Bp stars to derive some information on their

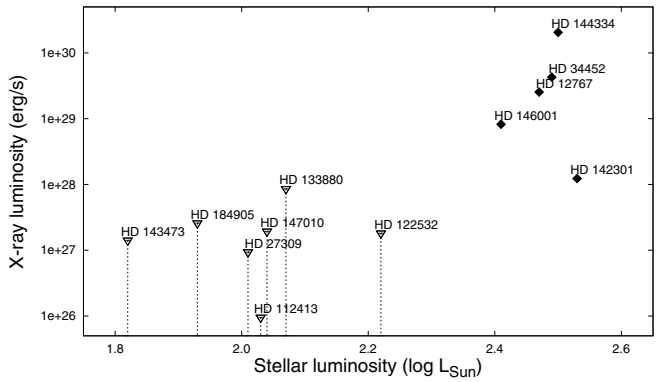

Fig. 8. X-ray vs. bolometric luminosity of the A0p stars IQ Aur (HD 34452) and α^2 CVn (HD 112413) compared to other Ap/Bp stars. X-ray detected stars are plotted as diamonds, upper limits are indicated by open triangles.

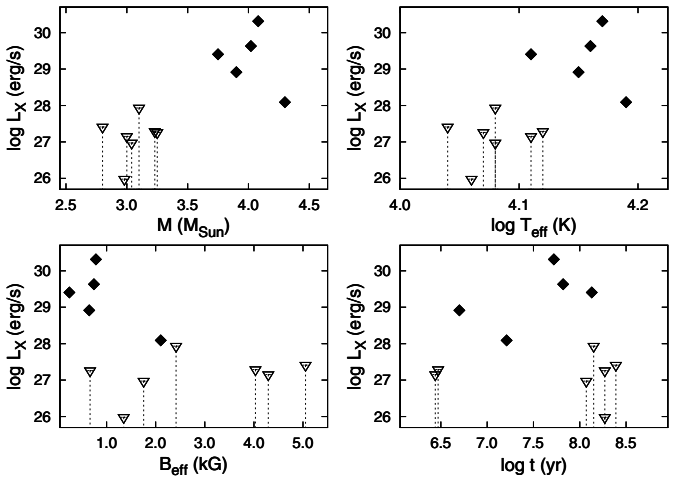

Fig. 9. Correlations for early-Ap/late-Bp stars, L_X vs. stellar mass, eff. temperature, eff. magnetic field and age (symbols as in Fig. 8).

Table 4. X-ray observations of the comparison Ap/Bp stars.

Target	Sp.type	Dist. (pc)	Instr./Obs.ID	Dur. (ks)	log L_X (erg s^{-1})
HD 12767	B9.5 Si	110	ACIS-S (5391)	3	29.4
HD 27309	A0 SiCr	96	XMM (0201360201)	41	<27.0
HD 122532	B9 Si	169	XMM (0302900101)	130	<27.3
HD 133880	B9 Si	126	ACIS-I (2543)	3	<28.0
HD 142301	B8IIIp	139	XMM (0142630301)	20	28.1
HD 143473	B9 Si	123	ACIS-S (5385)	15	<27.2
HD 144334	B8 Si He-w	149	ACIS-S (5393)	3	30.3
HD 146001	B8 He-w	140	ACIS-S (5394)	3	28.9
HD 147010	B9 SiCrFeSr	143	ACIS-S (5386)	15	<27.3
HD 184905	A0 SiSrCr	165	ACIS-S (5387)	15	<27.4

general X-ray properties. As a comparison sample we choose late-B to early-A magnetic CP stars with well determined distance and stellar parameter that are either likely single stars or spatially resolved in X-rays, although undiscovered binaries in the sample are not ruled out. However, their contribution is likely minor, because even the overall fraction of close, i.e., spectroscopic, binaries in Ap stars of CP2/Si type is with ∼20% significantly lower than those in non-magnetic stars (Abt & Snowden 1973). The comparison sample is specified in Table 4; some of these objects have already been presented, albeit with a different focus in Stelzer et al. (2006); Czesla & Schmitt (2007). Most stars are Si-stars, but some of the hotter ones are also classified as He-weak, moreover all stars have detected magnetic fields of a few hundred G up to several kG (Bychkov et al. 2003). The used stellar data are again taken from Kochukhov & Bagnulo (2006), additional values are from Landstreet et al. (2007). In Fig. 8 we show a comparison between the X-ray brightness and the stellar bolometric luminosity, errors are moderate, e.g. on $\log L_{\rm bol} \sim 0.1$. The comparison sample reveals a striking similarity to our findings for IQ Aur and α^2 CVn; either the stars are X-ray bright with predominantly $\log L_X \gtrsim 29.0$ erg s^{-1} or X-ray faint with most upper limits being around $\log L_X \lesssim 27.5$ erg s^{-1}, depending on the sensitivity of the respective exposure. Only high-luminosity objects are detected in X-rays, supporting an intrinsic X-ray generating mechanism. Furthermore, all stars with a high luminosity are detected as X-ray sources without exception. Statistically, the KS-probability of identical underlying distributions is well below 1% for our sample. A very similar dependence is present when using stellar mass, which is obviously related to luminosity; but notably we find that the strength of the magnetic field or the stellar age do not play a major role in making an Ap/Bp star an X-ray source (see Fig. 9). Unfortunately, the sample does not cover the full parameter space, for example it lacks stars in the mass range 3.3–3.8 $M_\odot$ or with magnetic fields of $B_{\rm eff} > 5$ kG and its size is still quite small. It therefore does not allow us to put strong constraints on the presence of a possible time-variability of the X-ray emission, but that we detected all stars above a stellar luminosity of around 200 $L_\odot$ (or 3.6 $M_\odot$) and none below suggests that a possible transient aspect of the MCWS phenomenon might be less important. However, as is also obvious from Figs. 8 and 9, the X-ray luminosities of the detected stars have a large spread, indicating that other parameters play an additional role in determining the specific X-ray properties of the individual stars.

5.4. Where does the X-ray emission of IQ Aur come from?

The *XMM-Newton* observation clearly shows that the plasma temperatures of IQ Aur are significantly higher than those estimated from the ROSAT data, where only weak indications for a hot component were found. This is very relevant for the MCWS model, because $T_X \propto V_{\rm sh}^2$ and consequently high wind speeds and a strong magnetic confinement must be present. Temperatures of about 10 MK require typical shock velocities of several hundred up to 1000 km s^{-1}. These values might be hard to obtain for A0p stars, though relatively high shock temperatures would be a natural explanation for the absence or weakness of a plasma excess at 2 MK. The relatively high O VIII/O VII ratio in IQ Aur could be explained by a quite high temperature in the colliding wind shocks of Ap stars; for example at shock speeds of 500–600 km s^{-1} no O VII excess emission is produced at all. At a few stellar radii a line-driven wind already has nearly its terminal speed, and for strong magnetic confinement a large longitudinal velocity component is expected to be present, easily explaining the absence of a cool excess even in a wind shock scenario. Similarly, the X-ray luminosity of IQ Aur requires a quite high mass loss rate and a very efficient conversion of kinetic wind energy to X-ray emission. While not implausible, this requires IQ Aur to drive a strong, fast wind. However, given the presence of a disk, a fraction of the harder X-ray emission could be generated in minor reconnection events. The O VII f/i-ratio diagnostic indicates that the X-ray emitting plasma is not exposed to strong UV radiation. Thus, if not shielded by an unknown medium, the

X-ray emitting regions are not predominantly close to the stellar surface, but have to be located at distances of several stellar radii.

Our lower limit derived of from the X-ray spectra of $d \approx 5\,R_*$ matches the value derived above for the inner disk radius, therefore a disk-like confinement region at distances of 5–15 R_* is a suitable candidate for the X-ray emitting region. On the other hand, the absence of significant rotational modulation over half of a rotation period implies that the changing viewing geometry introduces a negligible amount of time-variable, intervening material in the line of sight, caused either by an optically thick disk or the star itself. While the star as occulter appears unlikely given the large separation to the X-ray location, also rotational modulation is only expected for a disk if it is thick and the viewing angle changes significantly with phase. A small inclination is unlikely, given the relatively large $V \sin i$ for an A0p star. However, if the magnetic obliquity is small, rotational modulation effects are expected to be only minor. In this case the inclination should be quite large and the system would be viewed nearly edge-on at all times.

A strong flare-like event with 100 MK plasma is not expected to be produced by wind shocks even for magnetically channeled winds, thus these X-rays must be generated by magnetic reconnection. X-ray emitting structures on the surface of IQ Aur appear unlikely given the result from the X-ray diagnostics; additionally the magnetic field of Ap/Bp stars is overall a large-scale one and structurally differs from coronae where most X-ray plasma is confined in small-scale structures. Therefore the flare requires the presence of a rigidly rotating equatorial disk in the MCWS scenario, as predicted by the above outlined MHD simulations (ud-Doula et al. 2008). In this scenario magnetic reconnection occurs, leading to the production of hot X-ray emitting plasma and additionally, episodic centrifugal breakouts of confined plasma produce flare-like events, which were originally proposed to explain X-ray flares on the Bp star σ Ori (see discussion below, and ud-Doula et al. 2006). In contrast to coronal flares, these magnetic reconnection events are driven by centrifugal mass ejections that disrupt outer disk regions. During breakout, the centrifugal forces on the accumulated disk matter stretch the field lines more and more outward and finally reconnection occurs. The event is accompanied by the ejection of outer disk mass, an inward-propagating rebound and releases sufficient energy to produce hard X-ray flares. The finding of metallicity changes during the flare implies that the accumulated material in the circumstellar disk, which is heated during the disruption, is more metal-rich compared to the plasma that generates the QQ X-ray emission. Our rough estimates of the size of the flaring structure would imply that the outbreak-flare from IQ Aur was a more local event in the disk, involving a large clump or segment rather than the entire disk. Subsequent energy release or a change in the inner disk structure might be responsible for the flattening of the flare decay and the continuously enhanced level of X-ray emission after the event. Overall, this scenario appears suitable also to explain the flare event on IQ Aur. In this case, we have likely observed the first X-ray flare from an A0p star.

5.5. X-ray bright companions for Ap/Bp stars?

As an alternative explanation, it has been postulated that X-ray detected intermediate mass stars possess unknown late-type companions that actually produce the X-ray emission. Considering the estimated age of IQ Aur, i.e., several ten up to hundred Myr and comparing its X-ray luminosity with studies of the 70 Myr old Pleiades (Micela et al. 1996), an active G or early-K dwarf as well as an M dwarf binary would be suitable candidate X-ray sources. However, young active stars have typically significantly higher plasma temperatures than observed for IQ Aur (see, e.g. Güdel 2004) and their X-ray light curves show quite frequent X-ray flares of factor up to a few, whereas IQ Aur is dominated by softer emission (Fig. 7) and exhibits only minor variability except for the large flare. Other properties like the high f/i-ratio in the O VII triplet could be easily explained with a companion, typical densities are usually low and already a distance of 0.1 AU to IQ Aur would be in sufficient to completely erase the influence of the UV-field. The occurrence of a large flare is no problem either for an active late-type companion and the associated abundance changes are reminiscent of the chromospheric evaporation scenario describing the flare evolution.

Another criterion to consider is that IQ Aur is also a bright radio source at 6 cm with $\log L_6 \approx 16$ erg s^{-1} Hz^{-1}, whereas α^2 CVn with $\log L_6 < 14.9$ erg s^{-1} Hz^{-1} is radio dark (radio properties from Linsky et al. 1992). Because a tight correlation between X-ray and radio brightness measured at $\nu \gtrsim 5$ GHz is present for coronal sources, these measurements allow us to test the companion scenario by checking the well established X-ray/microwave(radio) correlation (also known as Güdel-Benz relation), which predicts $L_X/L_R = 10^{15.5\pm0.5}$ Hz for magnetically active stars (Güdel & Benz 1993). With a QQ X-ray luminosity of $\log L_X \approx 29.6$ erg s^{-1}, IQ Aur is radio-overluminous by roughly two orders of magnitude and consequently significantly violates this correlation. The deviation is well in excess of the generally observed scatter of the correlation that is typically of a factor of a few. Note that similar X-ray and radio fluxes were repeatedly observed for IQ Aur, making intrinsic variability quite unlikely to be the reason for the discrepancy. Also the B8p He-w/Si star HD 144334 (V 929 Sco) with $\log L_6 \approx 16.0$ erg s^{-1} Hz^{-1} and $\log L_X \approx 30.3$ erg/s violates the Güdel-Benz relation by one to two orders of magnitude, similar to the B8V He-w star HD 146001 with a radio detection at $\log L_6 \approx 16.0$ erg s^{-1} Hz^{-1} (plus one U.L. at $\log L_6 \lesssim 15.9$ erg s^{-1} Hz^{-1}). An even stronger violation is observed for the B8IIIp He-w/Si star HD 142301 (V 927 Sco), with $\log L_6 \approx 17.1$ erg s^{-1} Hz^{-1} and $\log L_X \approx 28.1$ erg s^{-1}, this star is radio overluminous by more than four orders of magnitude. On the other hand, all non X-ray detected comparison stars studied by Linsky et al. (1992), i.e., HD 122532, HD 147010, remained undetected as well at radio wavelengths at a limit of $\log L_6 \lesssim 15.7$ erg s^{-1} Hz^{-1}. This points to a joint occurrence of strong X-ray and radio emission for the sample stars. The fact that IQ Aur and all other X-ray detected Ap/Bp stars violate the Güdel-Benz relation by orders of magnitudes suggests that their emission does not originate in late-type dwarfs, but a contributing companion in individual objects is not ruled out.

5.6. What about hotter magnetic stars?

The MCWS model has also been applied to a variety of hotter stars, and it is illustrative to compare these with IQ Aur. A well studied example is the magnetic O5 star θ^1 Ori C, where Gagné et al. (2005) find that the dynamic MCWS model describes the X-ray properties of the star very well. It has an average X-ray luminosity of $L_X = 1\times10^{33}$ erg s^{-1} and using among other diagnostics f/i-line ratios, they conclude that the X-ray emitting plasma is located at distances of only $0.2 \ldots 0.5\,R_*$, i.e., quite close to the surface of the star. θ^1 Ori C exhibits rotational modulated X-ray emission, because it is a tilted magnetic rotator with $i = 45°$ and $\beta = 42°$, leading to a strong viewing-angle-dependent

visibility and obscuration of the X-ray emitting torus. θ^1 Ori C shows relatively hard X-ray emission from very hot plasma at temperatures of up to 30 MK, but no strong flaring. Noteworthy, there have also been reports of X-ray flares on early type magnetic stars, a prominent example is the B2p star σ Ori E. While Groote & Schmitt (2004) attribute a flare seen with ROSAT to σ Ori E itself, Sanz-Forcada et al. (2004) report a long duration (>10 h) flare with a count-rate increase by a factor of ten in an *XMM-Newton* observation and concluded that this more likely originates in a companion. They derived a QQ X-ray luminosity of $L_X = 9 \times 10^{30}$ erg s^{-1} and plasma temperatures up to 10–15 MK for σ Ori E. Also non CP, magnetic early-B stars are X-ray sources, e.g. the B0.2 star τ Sco with $L_X = 2 \times 10^{31}$ erg s^{-1} (Cohen et al. 2003). The *Chandra* spectra show emission lines that are broader than for coronal sources, but surprisingly narrow for a stellar wind shock scenario; together with the presence of hard emission and X-ray plasma locations at several stellar radii also make τ Sco a candidate for MCWS generated X-ray emission. Another example is the pulsating, hot magnetic giant star β Cep, where Favata et al. (2009) again find a good agreement between the predictions from the dynamic MCWS model and X-ray observations. It does again exhibit no flares, and with temperatures well below 10 MK the X-ray emission is remarkably soft, despite its X-ray brightness of $\log L_X = 4 \times 10^{30}$ erg s^{-1}. The authors derive distances of $\approx 5\ R_*$ as the most likely location of the cooler X-ray emitting material, while the hotter plasma is likely closer to the star. Because β Cep has $i = 45$ and $\beta = 85°$ but shows only minor modulation in its X-ray light curve, the authors exclude the presence of a thick disk and attribute the X-ray emission exclusively to magnetically channeled wind shocks.

When comparing IQ Aur to the above mentioned massive magnetic stars, we find some similarities and overall trends. Clearly, in general the X-ray luminosity decreases toward less massive stars, but all magnetic stars are X-ray overluminous with $\log L_X/L_{bol} \approx -6$ compared to similar "normal" massive stars. The bulk of the X-ray emitting plasma is located farther away from the central star, going from O over B to A-type stars and likely in the direction of increasing η_*. IQ Aur is also by far the coolest object and the only star in this comparison, where the f/i ratio of O VII is high. Comparing the X-ray temperatures, we find that the plasma on IQ Aur is cooler than on θ^1 Ori C, comparable to σ Ori E, but hotter than on β Cep. For stars with a moderate wind speed well below 1000 km s^{-1}, in the MCWS scenario the lower temperature plasma ($\lesssim$5 MK) is predominantly produced by wind shocks, whereas hotter plasma ($\gtrsim$10 MK) is generated by reconnection in the disk. Notably, the strong flaring sources IQ Aur and σ Ori E have by far the largest confinement parameter ($\log \eta_* \sim 6 \ldots 7$), favoring the effective accumulation of matter in the equatorial region and consequently breakout events. As shown in Fig. 10, their QQ spectra are also very similar, although the underlying stars differ significantly and σ Ori E has a twenty times higher X-ray luminosity.

5.7. The Ap/Bp star X-ray puzzle

Our findings provide some clear hints for the solution to the X-ray puzzle of A0p stars. We do not find strong support for the hypothesis that the X-ray emission of Ap/Bp stars is produced by X-ray emitting companions, but cannot rule out that in some cases multiple sources contribute to the observed emission. It is much more likely that the X-rays originate from intrinsic emission mainly generated in magnetically channeled wind shocks. However, predominantly or even exclusively the more massive, high-luminosity stars appear as X-ray sources. These late B/early A stars drive a stellar wind with a sufficiently high mass loss rate, whereas other stellar properties such as the magnetic topology or orientation and transient phenomena primarily influence the details of their X-ray appearance. For very strong magnetic confinement, an equatorial disk structure forms, where magnetic reconnection and centrifugal breakout events occur that produce hard X-ray emission and occasional flare-like events.

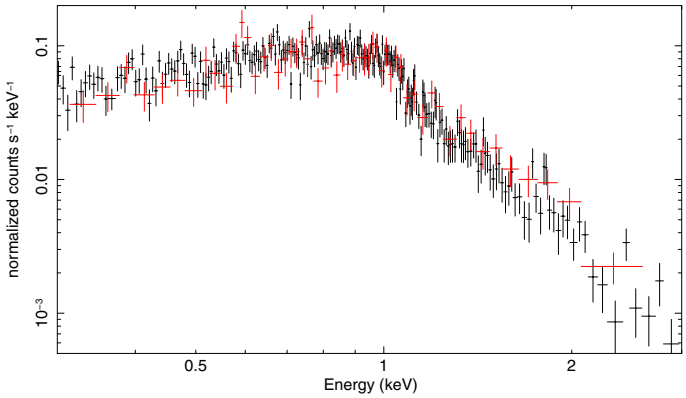

Fig. 10. Comparison of the quasi-quiescent X-ray spectra of the A0p star IQ Aur (black) and the B2p star σ Ori E (red) using XMM/PN data.

Dedicated modeling of A0p stars and their magnetically channeled winds, companion searches, and more extensive studies of similar objects are highly desired to gain even deeper insights into the origin of X-ray emission in these remarkable stars.

6. Summary and conclusions

Our main results can be summarized as follows:

1. We detect X-ray emission from IQ Aur at $\log L_X = 29.4$ erg s^{-1}, but failed to detect α^2 CVn at $\log L_X < 26$ erg s^{-1} although both are A0p stars. The QQ spectrum of IQ Aur exhibits significant emission from intermediate temperature and even hot plasma ($\gtrsim$10 MK), in addition to a strong cool component at 3 MK. The UV sensitive O VII f/i-ratio is high, therefore the X-ray emission very likely originates in regions at distances of $\gtrsim 5\ R_*$ above the stellar surface. The X-ray light curve shows minor variability without clear signs of a viewing-angle-dependent rotational modulation.
2. A massive X-ray flare with a rise time of about 1 ks and fast decay occurred during the IQ Aur observation. The X-ray luminosity at the flare peak is about $\log L_X = 31.5$ erg s^{-1} and plasma temperatures approach 100 MK. The flare originates in a fairly compact region and the metallicity of the X-ray emitting plasma increases significantly during the event.
3. Our X-ray data of IQ Aur can be reconciled within a dynamic MCWS model with strong magnetic confinement and build-up of a rigid disk where magnetic reconnection events occur. In this scenario, the flare-like event was produced by the centrifugal breakout of confined material. Alternatively, IQ Aur might be a multiple system where likely both components contribute to the observed X-ray emission.
4. Magnetically channeled stellar winds are the most promising explanation for the X-ray detection of Ap/Bp stars, although the presence of X-ray emission strongly depends on stellar parameters. A suitable quantity for setting the stage of MCWS generated X-rays appears to be a high stellar bolometric luminosity that supports a high mass loss, but

magnetic topology, orientation or transient phenomena also play a role in determining the specific X-ray properties of an individual Ap/Bp star.

Acknowledgements. This work is based on observations obtained with *Chandra* and *XMM-Newton*. J.R. acknowledges support from DLR under 50QR0803.

References

Abt, H. A., & Snowden, M. S. 1973, ApJS, 25, 137
Arnaud, K. A. 1996, in Astronomical Data Analysis Software and Systems V, ed. G. H. Jacoby, & J. Barnes, ASP Conf. Ser., 101, 17
Babel, J., & Montmerle, T. 1997, A&A, 323, 121
Berghoefer, T. W., Schmitt, J. H. M. M., Danner, R., & Cassinelli, J. P. 1997, A&A, 322, 167
Bohlender, D. A., Landstreet, J. D., & Thompson, I. B. 1993, A&A, 269, 355
Bychkov, V. D., Bychkova, L. V., & Madej, J. 2003, A&A, 407, 631
Cohen, D. H., de Messières, G. E., MacFarlane, J. J., et al. 2003, ApJ, 586, 495
Czesla, S., & Schmitt, J. H. H. M. 2007, A&A, 465, 493
Favata, F., Neiner, C., Testa, P., Hussain, G., & Sanz-Forcada, J. 2009, A&A, 495, 217
Gagné, M., Oksala, M. E., Cohen, D. H., et al. 2005, ApJ, 628, 986
Grevesse, N., & Sauval, A. J. 1998, Space Sci. Rev., 85, 161
Groote, D., & Schmitt, J. H. M. M. 2004, A&A, 418, 235
Güdel, M. 2004, A&ARv, 12, 71
Güdel, M., & Benz, A. O. 1993, ApJ, 405, L63
Günther, H. M., & Schmitt, J. H. M. M. 2009, A&A, 494, 1041
Hubrig, S., North, P., & Schöller, M. 2007, Astron. Nachr., 328, 475
Kochukhov, O., & Bagnulo, S. 2006, A&A, 450, 763
Kochukhov, O., & Wade, G. A. 2010, A&A, 513, A13
Landstreet, J. D. 1992, A&ARv, 4, 35
Landstreet, J. D., Bagnulo, S., Andretta, V., et al. 2007, A&A, 470, 685
Linsky, J. L., Drake, S. A., & Bastian, T. S. 1992, ApJ, 393, 341
Mewe, R., & Schrijver, J. 1978, A&A, 65, 99
Micela, G., Sciortino, S., Kashyap, V., Harnden, Jr., F. R., & Rosner, R. 1996, ApJS, 102, 75
Ness, J.-U., & Wichmann, R. 2002, Astron. Nachr., 323, 129
Porquet, D., Mewe, R., Dubau, J., Raassen, A. J. J., & Kaastra, J. S. 2001, A&A, 376, 1113
Preston, G. W. 1974, ARA&A, 12, 257
Reale, F. 2007, A&A, 471, 271
Reale, F., Betta, R., Peres, G., Serio, S., & McTiernan, J. 1997, A&A, 325, 782
Robrade, J., & Schmitt, J. H. M. M. 2007, A&A, 473, 229
Robrade, J., & Schmitt, J. H. M. M. 2009, A&A, 497, 511
Sanz-Forcada, J., Franciosini, E., & Pallavicini, R. 2004, A&A, 421, 715
Schmitt, J. H. M. M. 1997, A&A, 318, 215
Schmitt, J. H. M. M., & Kürster, M. 1993, Science, 262, 215
Schmitt, J. H. M. M., Golub, L., Harnden, Jr., F. R., et al. 1985, ApJ, 290, 307
Schröder, C., & Schmitt, J. H. M. M. 2007, A&A, 475, 677
Stelzer, B., Huélamo, N., Micela, G., & Hubrig, S. 2006, A&A, 452, 1001
Stelzer, B., Robrade, J., Schmitt, J. H. M. M., & Bouvier, J. 2009, A&A, 493, 1109
Townsend, R. H. D., & Owocki, S. P. 2005, MNRAS, 357, 251
ud-Doula, A., & Owocki, S. P. 2002, ApJ, 576, 413
ud-Doula, A., Townsend, R. H. D., & Owocki, S. P. 2006, ApJ, 640, L191
ud-Doula, A., Owocki, S. P., & Townsend, R. H. D. 2008, MNRAS, 385, 97